Electronic Supplementary Information

Fe-N-C electrocatalyst with dense active sites synthesized by expeditious pyrolysis of a natural Fe-N_4 macrocyclic complex

Minghao Wang[a,b], Bing Huang[a], Nannan Jiang[a], Tao Liu[a], Jianren Huang[a], Lunhui Guan*[a,b]

a. CAS Key Laboratory of Design and Assembly of Functional Nanostructures, and Fujian Provincial Key Laboratory of Nanomaterials, Fujian Institute of Research on the Structure of Matter, Chinese Academy of Sciences, Fuzhou, Fujian 350002, P.R. China
b. Fujian Normal University, Fuzhou 350108, Fujian, P.R. China.

* Corresponding Author: guanlh@fjirsm.ac.cn

Experimental section

1.1 Chemicals

Hemin (98%) and KOH (95%) were purchased from Meryer. Ketjen black (EC600JD) was purchased from Akzo Nobel N.V. Ammonium hydroxide (25 ~ 28%) was purchased from Tansoole. Pt/C (20 wt% and 40 wt%) was purchased from Suzhou sinero technology. Melamine (≥99.0%), urea (≥99.0%), Fe_2O_3 (≥99.0%), ethanol absolute (≥99.7%) and $HClO_4$ (70.0 ~ 72.0%) was purchased from Sinopharm Chemical Reagent Co.,Ltd. Deionized water was used throughout all the experiments. All reagents were used as received without any further purification. Carbon paper (HCP030N) was purchased from Toray Industries, Inc. Nafion 211 membrane and Nafion solution (D520) were purchased from Dupont.

1.2 Synthesis of N-KJB and g-C_3N_4

4 g of melamine and 1 g of Ketjen Black (KJB) were mixed by wet grinding with ethanol for 30 minutes, and then dried overnight in the oven at 80 **ºC**. Then the obtained powder was put into a tubular furnace and heated to 700 **ºC** for 30min (the heating rate is 10 **ºC** min^{-1}) under N_2 atmosphere, and then N-doped KJB is obtained denoted as N-

KJB. g-C_3N_4 was obtained by heating urea at 550 **ºC** for 3h in a muffle furnace in the ambient atmosphere.

1.3 Synthesis of Fe-KJB-3-60A

Firstly, 300 mg of N-KJB and 100 mg of g-C_3N_4 were dispersed in 30 ml of ethanol solution and then subjected to sonication for 2 hours. Afterwards, 210 mg of hemin was dissolved in 10 ml of ammonium hydroxide, then poured into the above solution and sonicated for 30 minutes. The suspension was poured into an evaporating dish and stirred at 70 **ºC** to evaporate the solvent. The resulting powder was further mixed by grinding. The homogeneous powder was filled into a customized hollow graphite rod and heated in a home-built low-voltage DC-current heating device at 60 A current for 1 min under vacuum.

1.4 Synthesis of control samples of Fe-KJB-1-60A, Fe-KJB-2-60A and Fe-KJB-4-60A

Except for the different amount of hemin added, other operation steps were identical to those for the synthesis of Fe-KJB-3-60A. The added amount of hemin in Fe-KJB-1-60A, Fe-KJB-2-60A, Fe-KJB-4-60A is 70 mg, 140 mg and 280 mg, respectively.

1.5 Synthesis of control samples of Fe-KJB-3-50A, Fe-KJB-3-70A, Fe-KJB-3-80A and Fe-KJB-3-900ºC

Fe-KJB-3-50A, Fe-KJB-3-70A and Fe-KJB-3-80A were synthesized by changing the heating current to 50A,70A and 80A, and other synthesis steps remained unchanged. As for Fe-KJB-3-900**ºC**, the homogeneous powder was carbonized at 900 **ºC** for 2 h (heating rate: 5 °C min^{-1}) under N_2 atmosphere in a tube furnace.

2. Sample Characterization

Transmission electron microscopy (TEM) and high-resolution TEM (HR-TEM) images were obtained by using the Tecnai F20 microscope. X-ray diffraction (XRD) measurements were performed with a Miniflex600 diffractometer using a Cu Kα (λ = 1.5405 Å) radiation source. Raman spectra were taken on a LabRAM HR spectrometer with 532 nm wavelength incident laser light. X-ray photoelectron spectroscopy (XPS)

analysis was performed on an ESCALAB 250Xi X-ray photoelectron spectrometer (Thermo, America). N_2 isothermal adsorption/desorption was recorded by a Brunauer-Emmett-Teller surface area analyzer (BET, Quantachrome Autoscorb-iQ2-XR) at 77K. Fe content in the synthesized samples was obtained Inductively Coupled Plasma Optical Emission Spectrometer (ICP-OES, Ultima-2), Fe-KJB-n-mA was dissolved by aqua regia solution.

3. Electrochemical Measurements

All of the electrochemical measurements were performed on a CHI 760D electrochemical station (Shanghai Chenhua, China) equipped with a conventional three-electrode system. The reference electrode was an Ag/AgCl electrode (saturated KCl), the counter electrode was a graphite rod electrode and the working electrode was a glassy carbon rotating disk electrode (GC-RDE) with a diameter of 5.0 mm, and 0.1 M KOH and 0.1 M $HClO_4$ as the alkaline and acidic electrolytes. All of the potentials reported in this work were calibrated to the reversible hydrogen electrode (RHE). Catalysts inks were prepared by dispersing 5 mg of catalyst in a solution of 950 μl isopropanol and 50 μl Nafion (5 wt%, Aldrich), and then applying sonication for 1 hour to form a uniform ink.

The working electrode was prepared through a drop casting strategy. 30 μl of the ink was loaded onto the GC electrode with a catalyst loading of ~0.765 mg cm^{-2}. But for commercial Pt/C (20 wt%) catalyst 4 μl of the ink was loaded onto the GC electrode with a catalyst loading of ~0.100 mg cm^{-2}. For the electrochemical ORR test, O_2 is first pumped into a 0.1 M KOH or 0.1 M $HClO_4$ aqueous solution for 30 minutes to reach oxygen saturation, and then a cyclic voltammeter (CV) scan was performed at 100 mV s^{-1} in the potential range of 0.164-1.164 V (in O_2-saturated 0.1 M KOH) or 0.056-1.056 V (in O_2-saturated 0.1 M $HClO_4$) until reaching a stable CV diagram. Then we conducted LSV tests within the same potential ranges as the CV measurements, at the sweep speed of 10mV s^{-1} and the rotation speed of 1600rpm. LSV and CV curves were also recorded under N_2 conditions and used to deduct the background.

Stability was examined by CV. The accelerated durability test (ADT) in alkaline medium was conducted in O_2-saturated 0.1 M KOH solution at a scan rate of 200 mV s^{-1} with the potential between 0.6 V and 1.0 V vs. RHE for 10000 cycles. The ADT in acid medium was conducted in O_2-saturated 0.1 M $HClO_4$ solution at a scan rate of 200 mV s^{-1} with the potential between 0.6 V and 1.0 V vs. RHE for 10000 cycles.

The kinetic current density (J_K) was calculated by Koutecky-Levich equation:

$$\frac{1}{J} = \frac{1}{J_K} + \frac{1}{J_L}$$

Where J_L and J is diffusion limited current density at 0.4 V (VS RHE) and the measured current density, respectively. It should be noted that the derived J_k is free of mass-transport ploaration. Then, we plotted the J_k and potential at Logarithmic scales. The straight line near the half-wave potential were used for linear fitting.

4. Liquid Zinc-air battery tests

All Zn-air batteries were evaluated under ambient conditions. The catalyst ink was prepared in the same way as for the ORR test above. For the Zn–air battery test, the air electrode was prepared by uniformly coating the as-prepared catalyst ink onto a circular carbon paper with a diameter of 2 cm, and the active area was a square with an area of 1 cm^2 in the center of the carbon paper, then drying at room temperature for 1 h. The mass loading was 0.15 mg cm^{-2}. But for commercial Pt/C catalyst the mass loading was 0.05 mg cm^{-2}. A Zn plate was used as the anode, and the catalyst loaded on carbon paper was used as the cathode. Both electrodes were assembled into a home-made Zn–air battery and a 6 M KOH aqueous solution with 0.2 M $(CH_3COO)_2$ Zn was used as the electrolyte to ensure reversible zinc electrochemical reactions at the anode. All data were collected from a CHI 760D electrochemical platform at room temperature, the polarization curves was recorded by LSV test at 10 mV s^{-1} in the potential range of 0.2-1.6 V.

5. Assemblies and tests of H_2-O_2 fuel cells

Cathode and anode catalyst inks were made by dispersing the catalyst in isopropanol to water (9:1) solvent mixture with Nafion (5 wt%) at an ionomer to catalysts ratio (I/C)

of 0.8, and then sonicated for 30 min. The catalyst-coated-membrane (CCM) with an area of 5 cm^2 was prepared by spraying ink on Nafion 211. The cathode catalyst load was 3 mg cm^{-2} and the anode catalyst (Pt/C, 40 wt%) load was 0.2 mg_{pt} cm^{-2}. The fabricated CCM was dried to completely evaporate the solvents. Two gas diffusion layers (GDLs), two gaskets, and the prepared CCM were pressed to obtain the membrane electrode assembly (MEA).

For H_2-O_2 single cell tests, 80% relative humidity and the cell temperature was maintained at 80 **ºC**. The backpressure was maintained at 1.5 bar, and the flow rates of H_2 and O_2 were 200 mL min^{-1} and 500 mL min^{-1} respectively. Prior to the data collection, an MEA activation was applied for 3 hours and then polarization curves of fuel cell were recorded by stepping voltages starting at 0.95V and decreasing by 5mV for 10 seconds until 0.3V by SMART2.

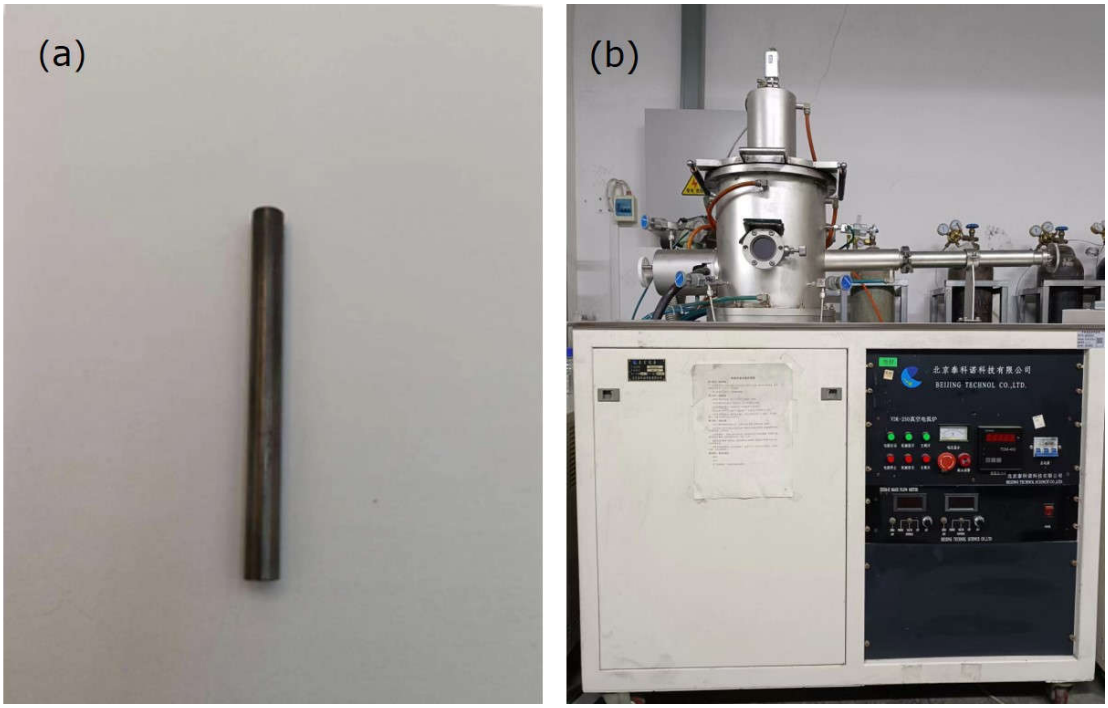

Fig. S1 Digital photographs of (a) the customized hollow graphite rod and (b) DC-current heating device.

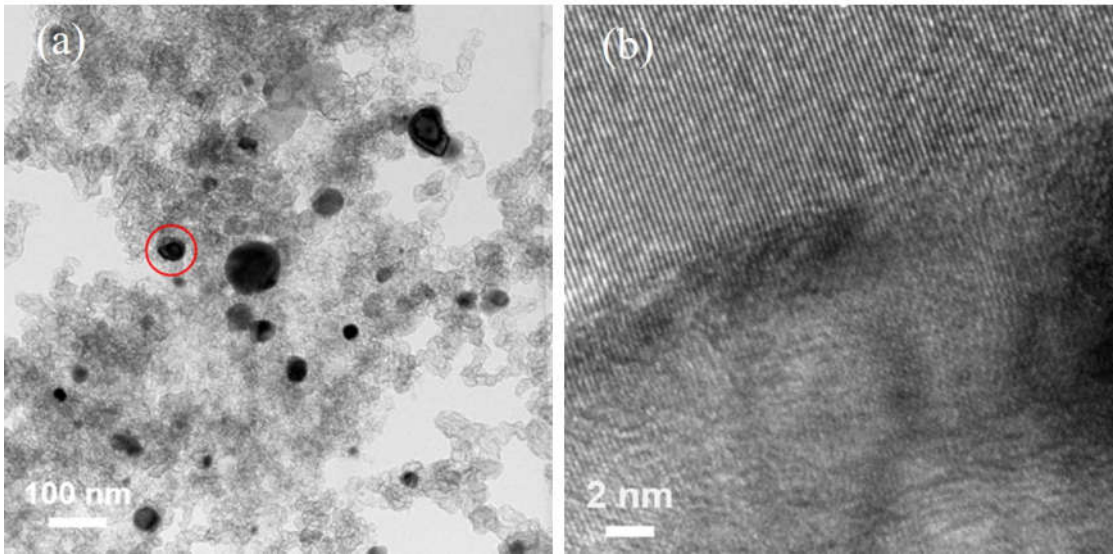

Fig.S2 TEM images of Fe-KJB-3-900ºC catalyst.

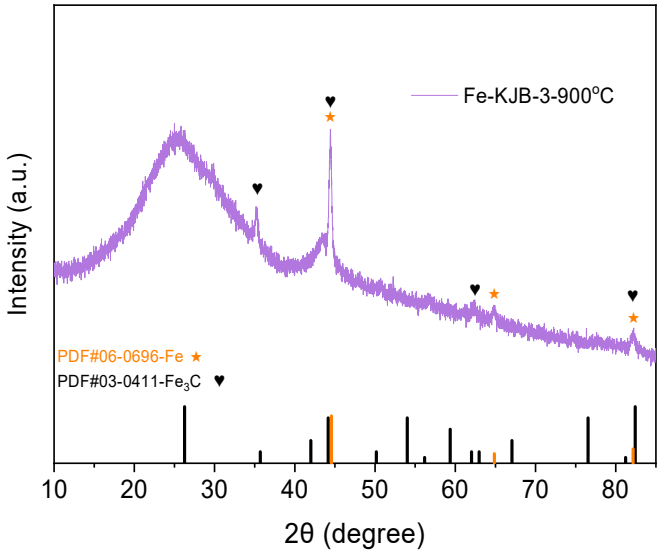

Fig.S3 XRD pattern of Fe-KJB-3-900ºC catalyst.

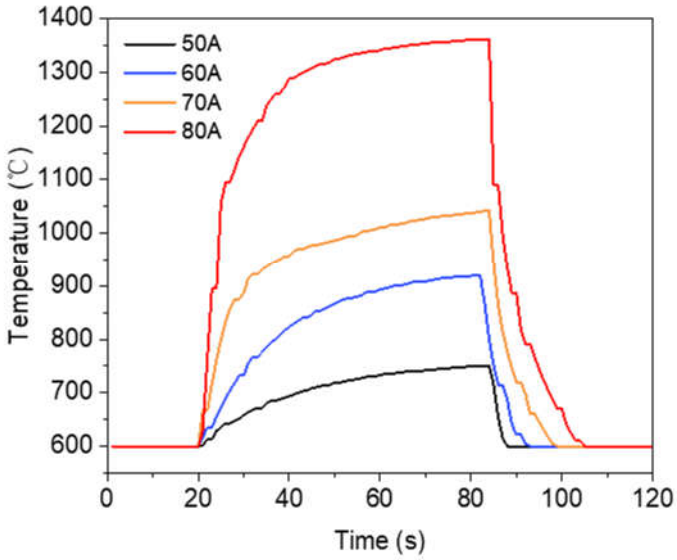

Fig.S4 The change of the temperature of the graphite rod with time at different currents.

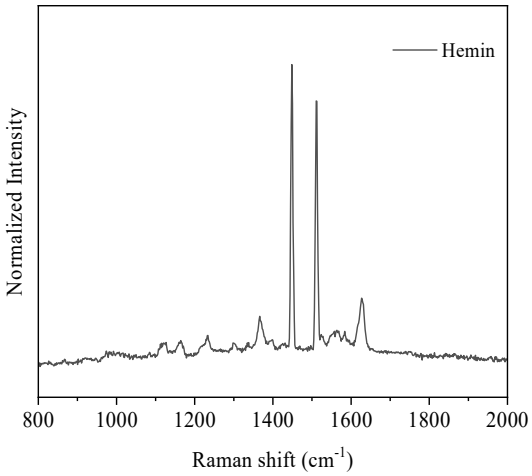

Fig. S5 Raman pattern of Hemin.

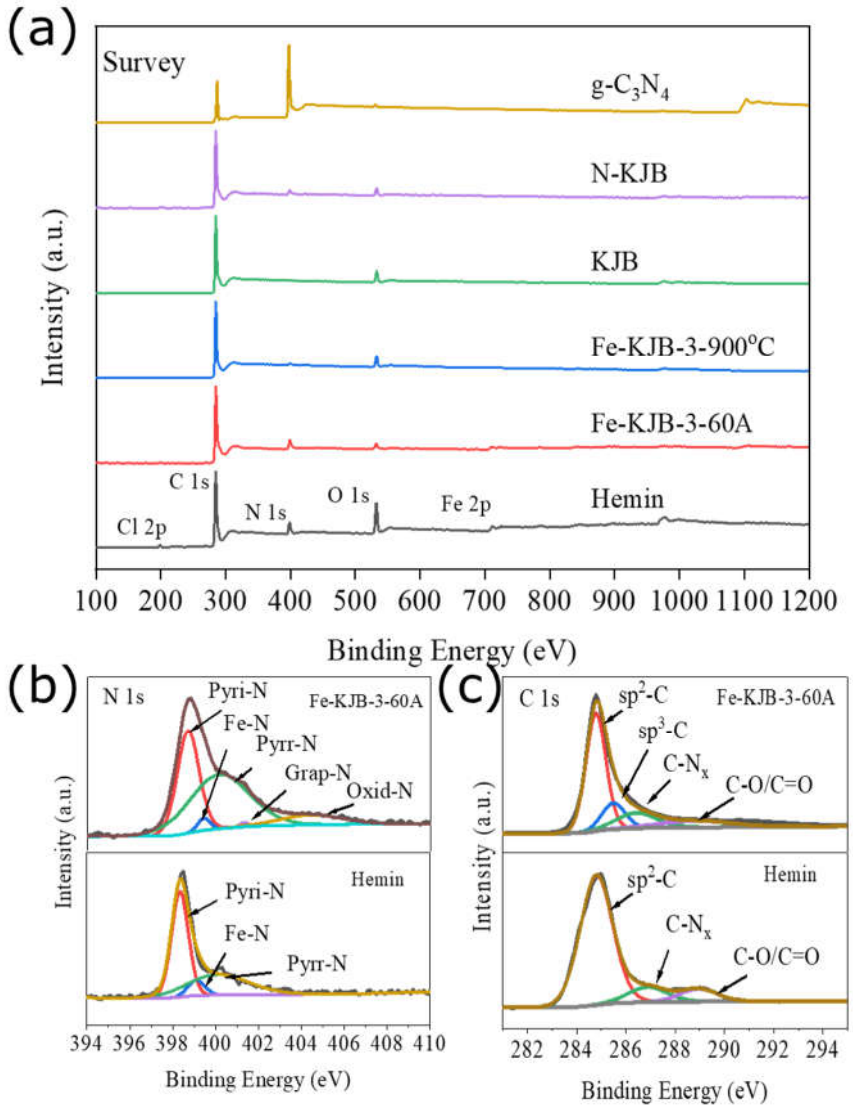

Fig.S6 (a) XPS survey spectra of Hemin, Fe-KJB-3-60A and Fe-KJB-3-900ºC, KJB, N-KJB, g-C_3N_4. High-resolution (b) N 1s and (c) C 1s XPS spectra of hemin and Fe-KJB-3-60A.

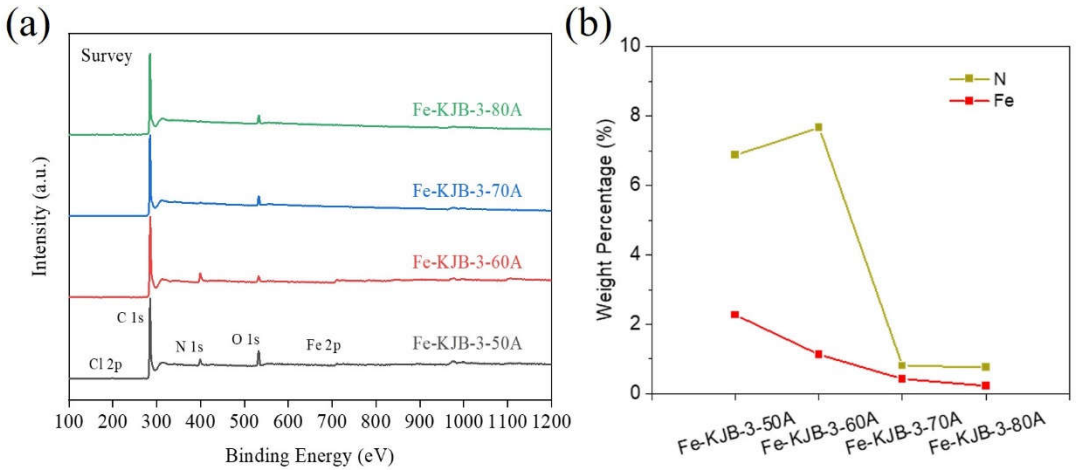

Fig.S7 (a) XPS Survey scans of Fe-KJB-3-50 A, Fe-KJB-3-60A, Fe-KJB-3-70 A and Fe-KJB-3-80 A. (b) N and Fe contents of the series catalysts synthesized by application of different Joule-heating currents, obtained from XPS spectra of Fe-KJB-3-50 A, Fe-KJB-3-60A, Fe-KJB-3-70 A and Fe-KJB-3-80 A.

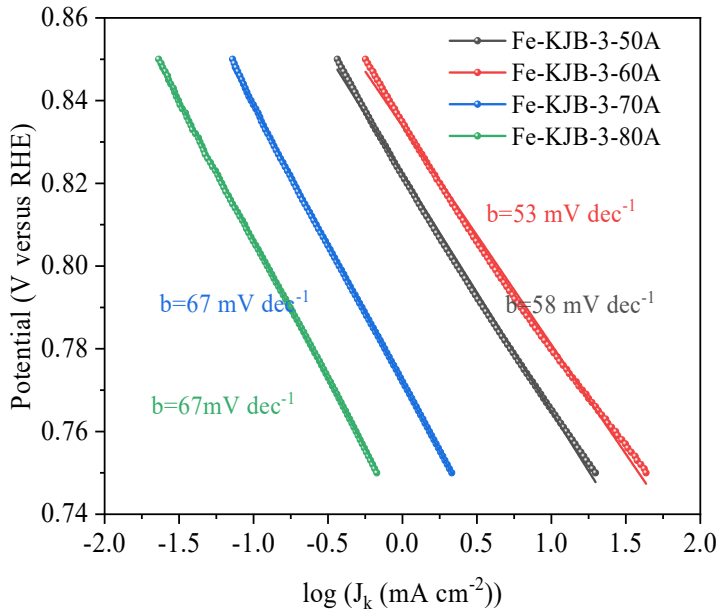

Fig.S8 Tafel plots of the catalysts synthesized under different current in O_2-saturated 0.1 M $HClO_4$ aqueous solution.

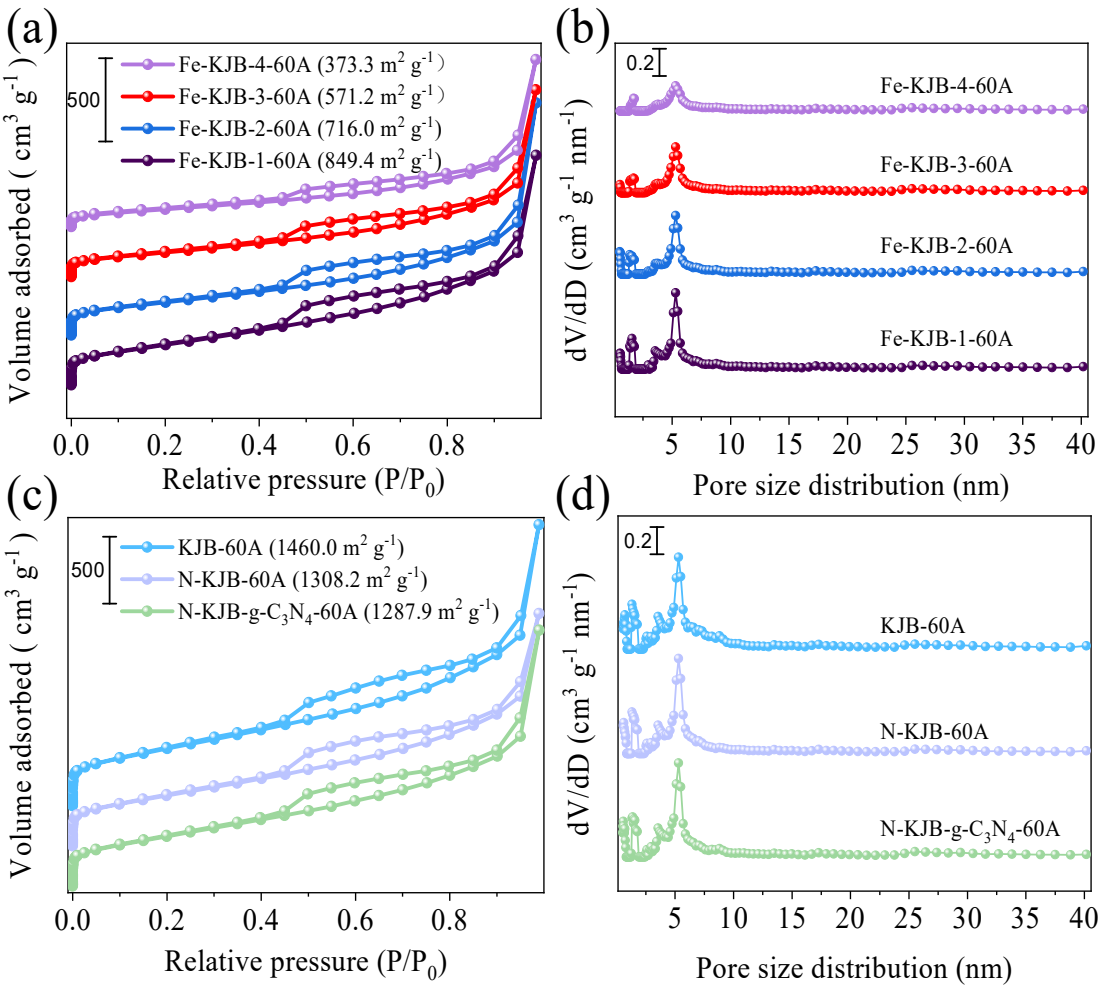

Fig.S9 (a),(c)N_2 adsorption–desorption isotherms; (b),(d) pore size distribution determined by the density functional theory (DFT) method of Fe-KJB-n-60A catalysts , KJB-60A, N-KJB-60A and N-KJB-g-C_3N_4-60A.

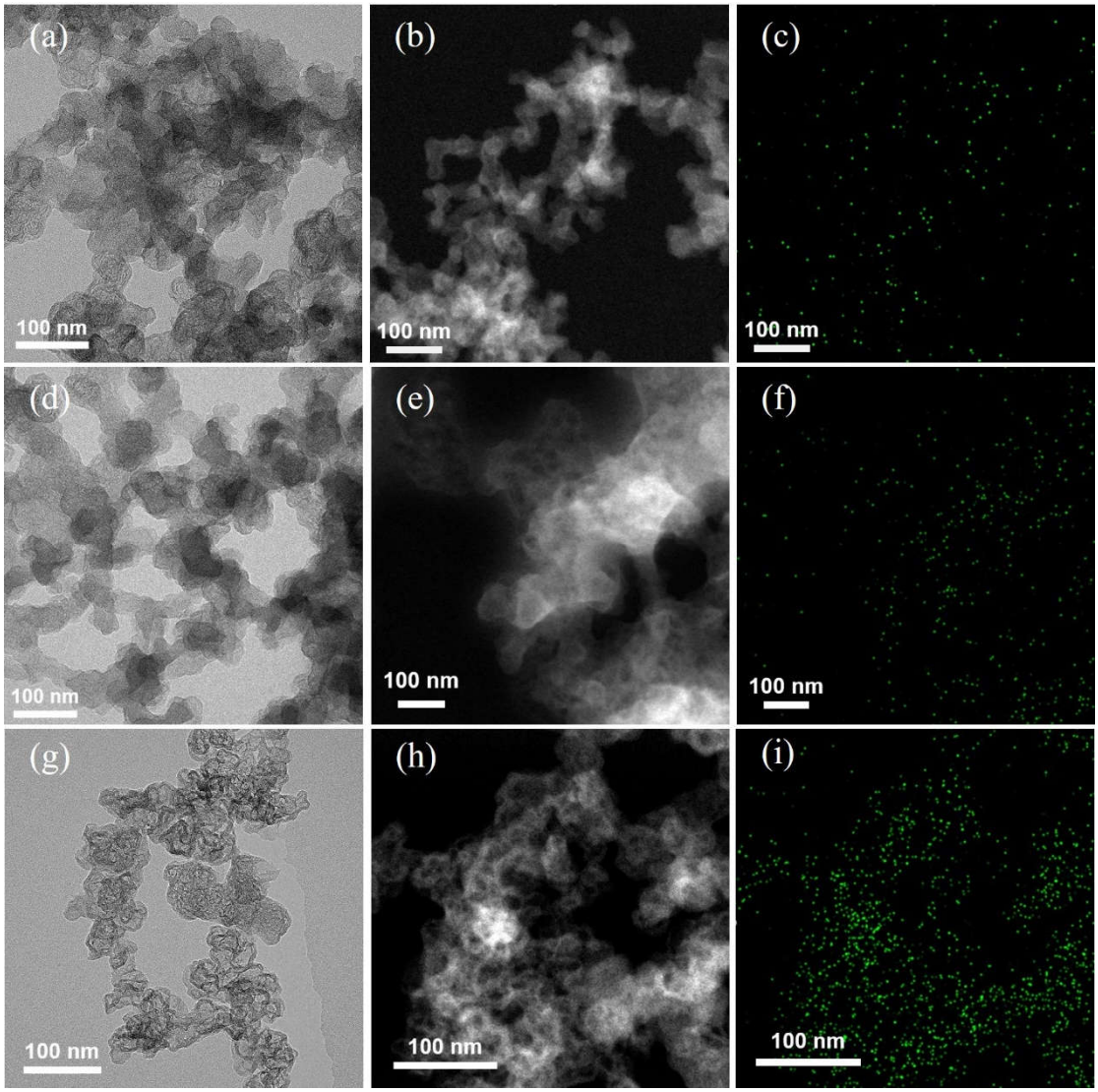

Fig.S10 TEM images, HAADF-STEM images and corresponding EDS elemental mapping images of Fe for: (a), (b), (c) of Fe-KJB-1-60A, (d), (e), (f)of Fe-KJB-2-60A, and (g), (h) and (i) of Fe-KJB-4-60A.

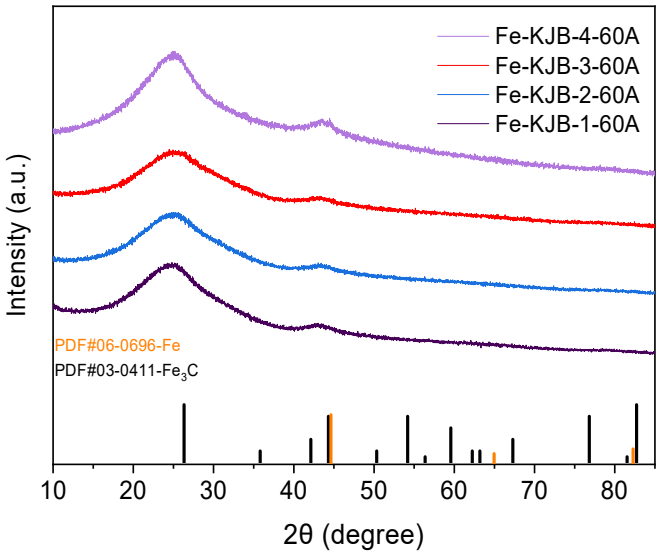

Fig.S11 XRD patterns of Fe-KJB-n-60A.

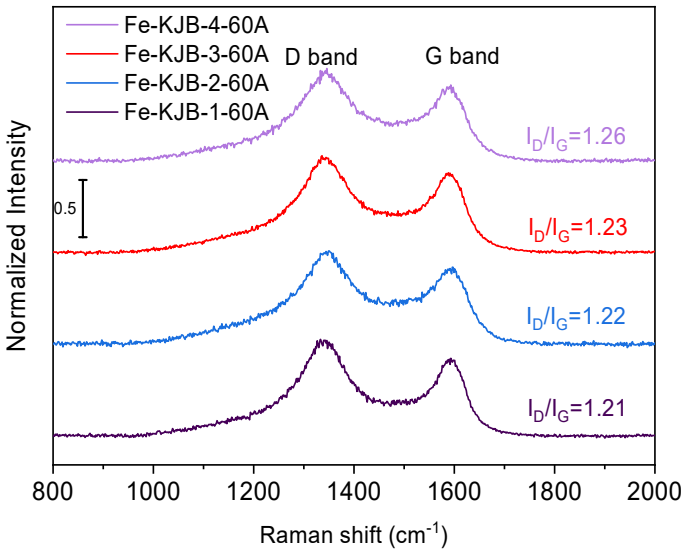

Fig.S12 Raman patterns of Fe-KJB-n-60A.

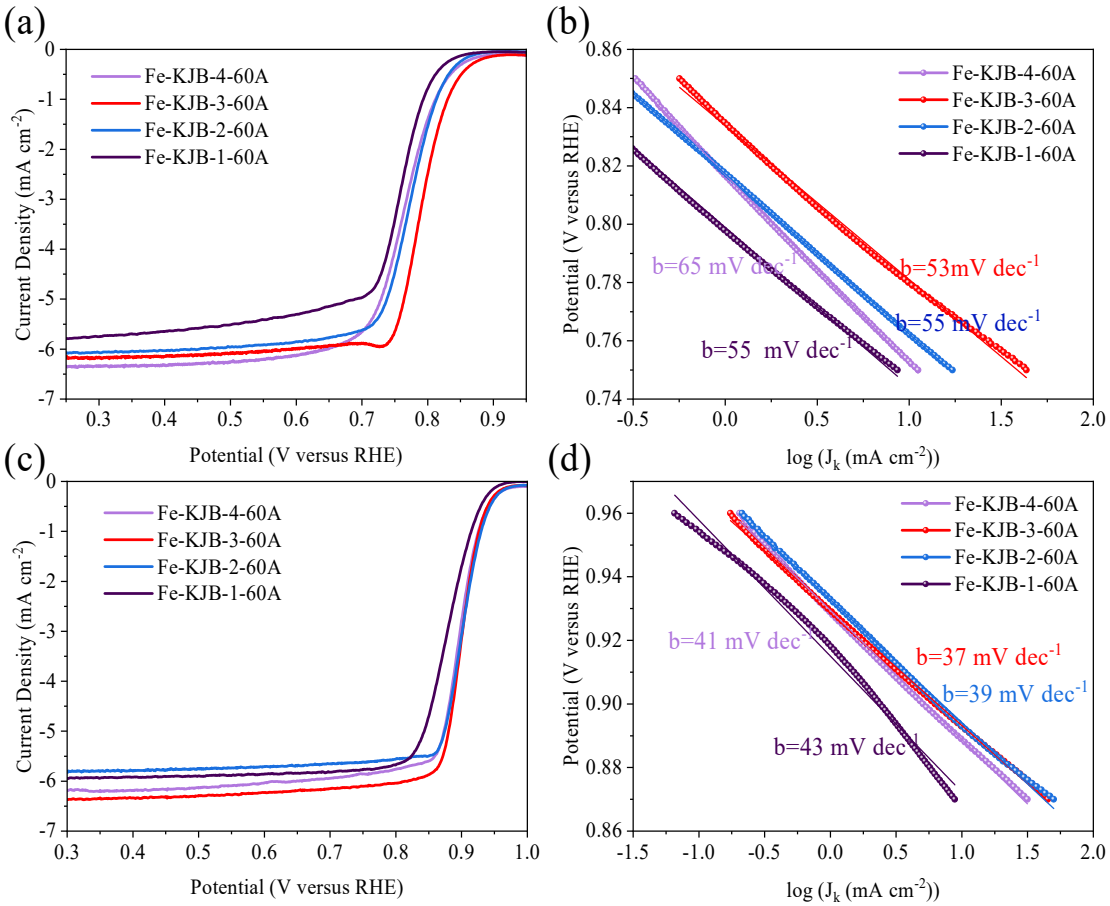

Fig.S13 LSV curves and corresponding Tafel plots of Fe-KJB-n-60A in: (a)and (b) in 0.1 M $HClO_4$ (c)and (d)in 0.1 M KOH.

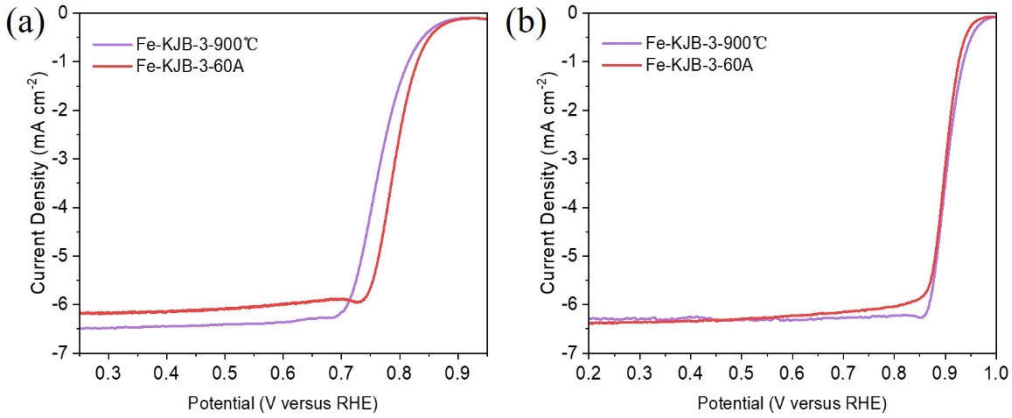

Fig.S14 LSV curves at 1600 rpm of Fe-KJB-3-60A and Fe-KJB-3-900 **ºC** (a) in 0.1 M $HClO_4$ aqueous solution (b) in 0.1 M KOH aqueous solution.

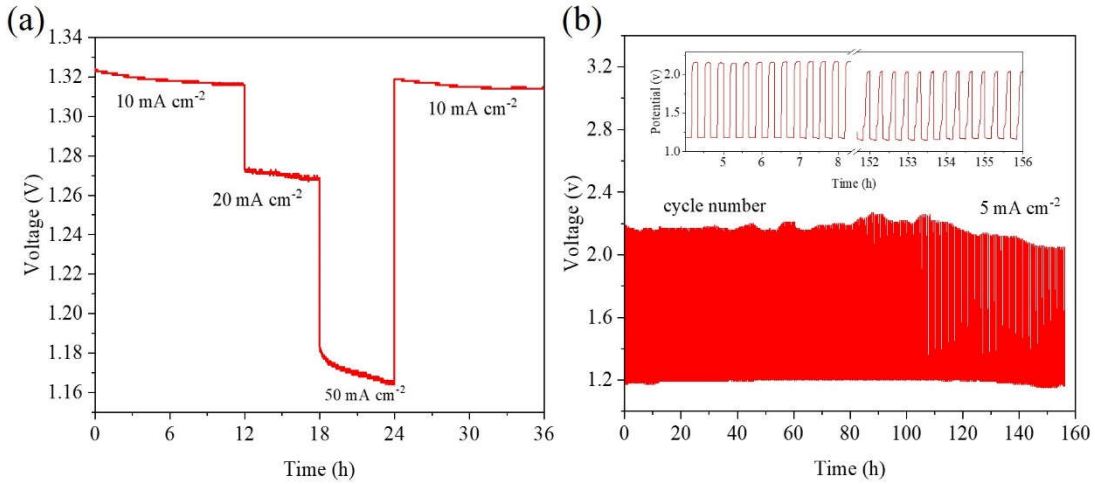

Fig.S15 (a) Galvanostatic discharge curves at different current densities, (b) Charge-discharge cycling performance at a constant charge-discharge current density of 5 mA cm^{-2} of the primary Zn-air battery with Fe-KJB-3-60A as the positive electrode catalyst.

Table. S1 ORR activities of various transition metal singe-atom electrocatalysts in acidic and alkaline conditions

catalysts	$E_{1/2}$ (V vs RHE in alkaline condition)	$E_{1/2}$ (V vs RHE in acidic condition)	Date source
Fe-KJB-3-60A	0.90	0.79	This work
Fe/SNCFs-NH_3[1]	0.89	-	Adv. Mater., 2021,34, 2105410
Fe(Fc)-N/S-C[2]	0.872	-	ACS Catal., 2021, 11, 7450-7459
commercial Fe–N–C[3]	0.846	-	Nat. Energy, 2021, 6, 834-843
Fe/NC-NaCl[4]	-	0.832	Adv. Energy Mater., 2021, 11，2100219
Fe− N−C−P/N,P−C[5]	0.87	0.80	ACS Catal., 2021, 11, 12754-12762
Fe/OES[6]	0.85	≈0.73*	Angew. Chem. Int. Ed., 2020, 59, 7384-7389
Fe-N/P-C-700[7]	0.867	0.72	J. Am. Chem. Soc., 2020, 142, 2404-2412
3DOM Fe–N–C-900[8]	0.875	0.784	Nano Energy, 2020, 71, 104547
Fe−N4−C-60[9]	-	0.80	Adv. Mater., 2020, 32, e2000966
Fe_{SA}–N–C[10]	0.90	0.80	Nat. Commun, 2020, 11, 2831
Co SANC-850[11]	0.863	-	J. Mater. Chem. A, 2020, 8, 2131-2139
Co-SAs@NC[12]	0.82	-	Angew. Chem. Int. Ed., 2019, 58, 5359-5364
Fe/N/S-PCNT[13]	0.84	0.62*	J. Mater. Chem. A, 2019, 7, 1607-1615
Fe-SAs/NSC[14]	0.87	≈0.7	J. Am. Chem. Soc., 2019, 141, 20118-20126
Co-SAs/NSC[14]	0.86	-	
Ni-SAs/NSC[14]	0.82	-	
Fe-NSDC[15]	0.84	0.74	Small, 2019, 15, e1900307
Co-N,B-CSs[16]	0.83	-	ACS Nano, 2018, 12, 1894-1901

Except "*" represent the E1/2 values measured in 0.5 M H_2SO_4 aqueous solution. The acidic condition refers to 0.1 M $HClO_4$ aqueous solution and the alkaline condition refers to 0.1 M KOH solution.

Table. S2 Specific surface aeras and weight percentage of Fe (determined by ICP-OES) of the series of catalysts synthesized by applying different Joule-heating currents.

Samples	Fe-KJB-3-50A	Fe-KJB-3-60A	Fe-KJB-3-70A	Fe-KJB-3-80A
S_a ($m^2 \cdot g^{-1}$)	512.7	571.2	592.1	517.3
Fe in the obtained catalysts (wt%)	2.35	3.08	1.35	1.49

Table. S3 Performance comparison of the liquid-state ZABs based on M-Nx/C (M = Fe, Co) catalysts.

Catalysts	Power density (mW cm^{-2})	Cycling condition (mA cm^{-2})	Cyclability evaluation	Charge/discharge voltage gaps (V) at a certain current density (mA cm^{-2})	Data source
Fe-KJB-3-60A	251	5	156 h	1.0 @ 5	This work
Fe/SNCFs-NH_3[1]	255.84	1	1000 h	0.78 @ 5	Adv. Mater., 2021, 34, 2105410
Fe–AC-2[17]	153	5	50 h	-	J. Mater. Chem. A, 2021, 9, 7137-7142
Fe,Co-SA/CS[18]	86.65	5	100 h	0.71 @ 5	Small Methods, 2021, 5, e2000751
Fe/OES	186.8	5	130 h	0.81 @ 10	Angew. Chem. Int. Ed., 2020, 59, 7384-7389
SA-Fe-NHPC[19]	266.4	20 (mechanically rechargeable)	240 (mechanically rechargeable)	-	Adv. Mater., 2020, 32, e1907399
Fe-N/P-C-700[7]	133.2	10	40 h	0.9 @ 10	J. Am. Chem. Soc., 2020, 142, 2404-2412
Co-SAs@NC[12]	105.3	10	85 h	0.85 @ 10	Angew. Chem. Int. Ed., 2019, 58, 5359-5364
Co/Co–N–C[20]	132	10	330 h	0.82 V@10	Adv. Mater., 2019, 31, e1901666
SCoNC[21]	194	5	20 h	-	Adv. Energy Mater., 2019, 9, 1900149
Fe-Nx-C[22]	96.4	5	30 h	0.803 @ 5	Adv. Funct. Mater., 2019, 29, 1808872

Fe-N4 SAs/NPC[23]	232	2	36 h	-	Angew. Chem. Int. Ed., 2018, 57, 8614-8618
NC-Co SA[24]	-	10	108 h	-	ACS Catal., 2018, 8, 8961-8969

References

1 L. Yang, X. Zhang, L. Yu, J. Hou, Z. Zhou and R. Lv, *Adv. Mater.*, 2021, **34**, 2105410.

2 X. Li, X. Yang, L. Liu, H. Zhao, Y. Li, H. Zhu, Y. Chen, S. Guo, Y. Liu, Q. Tan and G. Wu, *ACS Catal.*, 2021, **11**, 7450-7459.

3 H. Adabi, A. Shakouri, N. Ul Hassan, J. R. Varcoe, B. Zulevi, A. Serov, J. R. Regalbuto and W. E. Mustain, *Nat. Energy*, 2021, **6**, 834-843.

4 Q. Wang, Y. Yang, F. Sun, G. Chen, J. Wang, L. Peng, W. T. Chen, L. Shang, J. Zhao, D. Sun-Waterhouse, T. Zhang and G. I. N. Waterhouse, *Adv. Energy Mater.*, 2021, **11**, 2100219.

5 H. Yin, P. Yuan, B.-A. Lu, H. Xia, K. Guo, G. Yang, G. Qu, D. Xue, Y. Hu, J. Cheng, S. Mu and J.-N. Zhang, *ACS Catal.*, 2021, **11**, 12754-12762.

6 C. C. Hou, L. Zou, L. Sun, K. Zhang, Z. Liu, Y. Li, C. Li, R. Zou, J. Yu and Q. Xu, *Angew. Chem. Int. Ed.*, 2020, **59**, 7384-7389.

7 K. Yuan, D. Lutzenkirchen-Hecht, L. Li, L. Shuai, Y. Li, R. Cao, M. Qiu, X. Zhuang, M. K. H. Leung, Y. Chen and U. Scherf, *J. Am. Chem. Soc.*, 2020, **142**, 2404-2412.

8 X. Zhang, X. Han, Z. Jiang, J. Xu, L. Chen, Y. Xue, A. Nie, Z. Xie, Q. Kuang and L. Zheng, *Nano Energy*, 2020, **71**, 104547.

9 X. Wang, Y. Jia, X. Mao, D. Liu, W. He, J. Li, J. Liu, X. Yan, J. Chen, L. Song, A. Du and X. Yao, *Adv. Mater.*, 2020, **32**, e2000966.

10 L. Jiao, R. Zhang, G. Wan, W. Yang, X. Wan, H. Zhou, J. Shui, S. H. Yu and H. L. Jiang, *Nat. Commun*, 2020, **11**, 2831.

11 Y. Wang, B. Yu, K. Liu, X. Yang, M. Liu, T.-S. Chan, X. Qiu, J. Li and W. Li, *J. Mater. Chem. A*, 2020, **8**, 2131-2139.

12 X. Han, X. Ling, Y. Wang, T. Ma, C. Zhong, W. Hu and Y. Deng, *Angew. Chem. Int. Ed.*, 2019, **58**, 5359-5364.

13 Z. Tan, H. Li, Q. Feng, L. Jiang, H. Pan, Z. Huang, Q. Zhou, H. Zhou, S. Ma

and Y. Kuang, *J. Mater. Chem. A*, 2019, **7**, 1607-1615.

14 J. Zhang, Y. Zhao, C. Chen, Y. C. Huang, C. L. Dong, C. J. Chen, R. S. Liu, C. Wang, K. Yan, Y. Li and G. Wang, *J. Am. Chem. Soc.*, 2019, **141**, 20118-20126.

15 J. Zhang, M. Zhang, Y. Zeng, J. Chen, L. Qiu, H. Zhou, C. Sun, Y. Yu, C. Zhu and Z. Zhu, *Small*, 2019, **15**, e1900307.

16 Y. Guo, P. Yuan, J. Zhang, Y. Hu, I. S. Amiinu, X. Wang, J. Zhou, H. Xia, Z. Song, Q. Xu and S. Mu, *ACS Nano*, 2018, **12**, 1894-1901.

17 Y. Wang, Q. Li, L.-c. Zhang, Y. Wu, H. Chen, T. Li, M. Xu and S.-J. Bao, *J. Mater. Chem. A*, 2021, **9**, 7137-7142.

18 V. Jose, H. Hu, E. Edison, W. Manalastas, Jr., H. Ren, P. Kidkhunthod, S. Sreejith, A. Jayakumar, J. M. V. Nsanzimana, M. Srinivasan, J. Choi and J. M. Lee, *Small Methods*, 2021, **5**, e2000751.

19 G. Chen, P. Liu, Z. Liao, F. Sun, Y. He, H. Zhong, T. Zhang, E. Zschech, M. Chen, G. Wu, J. Zhang and X. Feng, *Adv. Mater.*, 2020, **32**, e1907399.

20 P. Yu, L. Wang, F. Sun, Y. Xie, X. Liu, J. Ma, X. Wang, C. Tian, J. Li and H. Fu, *Adv. Mater.*, 2019, **31**, e1901666.

21 J. Wu, H. Zhou, Q. Li, M. Chen, J. Wan, N. Zhang, L. Xiong, S. Li, B. Y. Xia, G. Feng, M. Liu and L. Huang, *Adv. Energy Mater.*, 2019, **9**, 1900149.

22 J. Han, X. Meng, L. Lu, J. Bian, Z. Li and C. Sun, *Adv. Funct. Mater.*, 2019, **29**, 1808872.

23 Y. Pan, S. Liu, K. Sun, X. Chen, B. Wang, K. Wu, X. Cao, W. C. Cheong, R. Shen, A. Han, Z. Chen, L. Zheng, J. Luo, Y. Lin, Y. Liu, D. Wang, Q. Peng, Q. Zhang, C. Chen and Y. Li, *Angew. Chem. Int. Ed.*, 2018, **57**, 8614-8618.

24 W. Zang, A. Sumboja, Y. Ma, H. Zhang, Y. Wu, S. Wu, H. Wu, Z. Liu, C. Guan, J. Wang and S. J. Pennycook, *ACS Catal.*, 2018, **8**, 8961-8969.